

BCS-BEC crossover in atomic Fermi gases in quasi-two-dimensional Lieb lattices: Effects of flat band and finite temperature

Hao Deng,^{1,2,3,*} Lin Sun,^{3,2,*} Chuping Li,^{1,2,3} Yuxuan Wu,^{1,2,3} Junru Wu,^{1,2,3} and Qijin Chen^{1,2,3,†}

¹*Hefei National Research Center for Physical Sciences at the Microscale and School of Physical Sciences, University of Science and Technology of China, Hefei, Anhui 230026, China*

²*Shanghai Research Center for Quantum Science and CAS Center for Excellence in Quantum Information and Quantum Physics, University of Science and Technology of China, Shanghai 201315, China*

³*Hefei National Laboratory, University of Science and Technology of China, Hefei 230088, China*

(Dated: January 9, 2024)

We investigate the finite-temperature superfluid behavior of ultracold atomic Fermi gases in quasi-two-dimensional Lieb lattices with a short-range attractive interaction, using a pairing fluctuation theory within the BCS-BEC crossover framework. We find that the presence of a flat band, along with van Hove singularities, leads to exotic quantum phenomena. As the Fermi level enters the flat band, both the gap and the superfluid transition temperature T_c as a function of interaction change from a conventional exponential behavior into an unusual power law, and the evolution of superfluid densities with temperature also follows a power law even at weak interactions. The quantum geometric effects, manifested by an enhanced effective pair hopping integral, may contribute significantly to both T_c and the superfluidities. As the chemical potential crosses the van Hove singularities in the weak interaction regime, the nature of pairing changes between particle-like and hole-like. A pair density wave state emerges at high densities with a relatively strong interaction strength.

I. INTRODUCTION

Ultracold atomic Fermi gases in optical lattices have garnered great interest in recent years due to the multiple adjustable parameters, which render them suitable for quantum simulations and quantum computation, as well as quantum engineering [1–3]. These parameters include interaction strength, lattice potential well depth, temperature, dimension, population imbalance, etc [4–7]. By tuning the interaction strength, a perfect crossover from a BCS type of superfluidity to Bose–Einstein condensation (BEC) of atomic pairs has been achieved [1, 8].

Using atomic Fermi gases in optical lattices, one can simulate, e.g., the Hubbard model [9], and study various (possibly exotic) quantum phenomena in strongly correlated systems, including the widespread pseudogap phenomenon in high-temperature superconductors [10–12]. In particular, models with flat bands have gained significant attention due to their high density of states and the potential for the enhancement of the superconducting transition temperature T_c , as well as the occurrence of quantum Hall states with nonzero Chern number [13–17]. Flat bands have been realized and studied in bipartite lattices, including Lieb lattice, perovskite lattice, and magic-angle twisted graphene superlattices, along with kagome and honeycomb lattices [13, 18–21]. Here we focus on the Lieb lattice, which has been realized in optical lattices of ultracold Fermi gases [22, 23]. The Lieb lattice is a line-centered square lattice with three bands, of which the upper and the lower band come into contact with the flat band in the form of Dirac points [24]. Numerous theoretical and experimental studies have been conducted on Lieb lattices [22, 23, 25], including investigations into the Chern number

in semimetals and attractive Hubbard models [26, 27], ferromagnetic and antiferromagnetic states in a repulsive Hubbard model [28–30], the superconductor-insulator transition [31], and the competition between pairing and charge density wave at half filling [32], as well as the effect of the next-nearest-neighbor hopping associated with spin-orbit coupling [17, 33–35]. The rich physics associated with Lieb lattices makes it crucial to study the superfluidity and pairing phenomenon of ultracold Fermi gases in a Lieb lattice. Our recent study on the ground-state of atomic Fermi gases in a quasi-two-dimensional Lieb lattice reveals that, within an attractive Hubbard model, the flat band has strong effects on the behavior of the pairing gap and in-plane superfluid density; as the Fermi level falls within the flat band, both exhibit an unusual power law dependence on the interaction strength. [36].

In this paper, we study the superfluid behavior of ultracold atomic Fermi gases in a quasi-two-dimensional Lieb lattice at finite temperature, and focus on a tight-binding model with attractive Hubbard interaction, which only involves nearest neighbor hopping and has a flat band with a zero Chern number [37]. Within the pairing fluctuation theory, we find that the presence of the flat band, along with van Hove singularities, has a strong influence on the superfluid properties of the system, leading to various exotic phenomena. When the Fermi level enters the flat band in the weak interaction regime, the dependence of both T_c and the pairing gap Δ on the interaction strength changes from an exponential behavior to an unusual power law, with a density-dependent exponent, indicating a significant departure from the conventional BCS-like behavior. Moreover, the temperature dependence of superfluid densities at weak interactions also follows a power law in the low temperature regime, rather than the conventional exponential dependence. In addition, both the effective pair hopping integral and superfluid densities exhibit important quantum geometric effects, which enhance the superfluidity. When the chemical potential exceeds the van Hove singularities in the lower band, it shows a nonmonotonic behavior as

* These authors contributed equally to this work.

† Corresponding author: qjc@ustc.edu.cn

a function of the interaction strength in the weak interaction regime, associated with the change from particle-like to hole-like pairing. Moreover, a pair density wave (PDW) ground state emerges at intermediate pairing strength for relatively large densities, as a consequence of strong inter-pair repulsive interactions and relatively large pair size at intermediate pairing strength, which is also found in dipolar Fermi gases [38] and Fermi gases in 2D optical lattice with 1D continuum dimension [39, 40].

II. THEORETICAL FORMALISM

A. The Hamiltonian

Here we consider a nearest-neighbor tight-binding model for ultracold Fermi gases with attractive Hubbard interaction in a quasi-two-dimensional Lieb lattice. The non-interacting Hamiltonian of a Lieb lattice under the orbital representation is given by

$$H_0 = \sum_{\mathbf{k}\sigma} \hat{c}_{\mathbf{k}\sigma}^\dagger \hat{H}_{\mathbf{k}} \hat{c}_{\mathbf{k}\sigma}$$

where $\hat{c}_{\mathbf{k}\sigma} = [C_{A\mathbf{k}\sigma}, C_{B\mathbf{k}\sigma}, C_{C\mathbf{k}\sigma}]^T$. The symbol A represents the lattice site in a standard square lattice with B and C located on every side of the square, as shown in Fig. 1A of Ref. [22]. This leads to the Hamiltonian in momentum space for free fermions

$$\hat{H}_{\mathbf{k}} = \begin{bmatrix} d_k & a_k & b_k \\ a_k & d_k & 0 \\ b_k & 0 & d_k \end{bmatrix},$$

where $a_k = 2t[1 - \cos(k_x/2)]$ and $b_k = 2t[1 - \cos(k_y/2)]$ represent the hopping in the x and y directions, respectively, and $d_k = 2t_z(1 - \cos k_z) - \mu$ the dispersion in the out-of-plane \hat{z} direction, with t and t_z being the in-plane and out-of-plane hopping integral, respectively. We use t as the unit of energy and take $t_z/t = 0.01$ for the quasi-two dimensionality. In this paper, we restrict $k_{i=x,y,z}$ within the first Brillouin zone, set the lattice constant $a = 1$, and measure the energy relative to the bottom of the lower energy band. Diagonalizing $\hat{H}_{\mathbf{k}}$ leads to three bands with dispersions $\xi_{\mathbf{k}}^\alpha = \alpha\sqrt{2t}\sqrt{2 + \cos k_x + \cos k_y} + 2\sqrt{2}t + 2t_z(1 - \cos k_z) - \mu$, where $\alpha = \pm, 0$ denotes the upper, the lower and the flat band, respectively. This yields H_0 in the band representation, $H_0 = \sum_{\mathbf{k}\alpha\sigma} \xi_{\mathbf{k}}^\alpha \hat{c}_{\mathbf{k}\alpha\sigma}^\dagger c_{\mathbf{k}\alpha\sigma}$, where $c_{\mathbf{k}\alpha\sigma}$ is the annihilation operator in band α .

The interaction Hamiltonian in the band representation is given by

$$H_{\text{int}} = \sum_{\mathbf{k}\mathbf{k}'\alpha\beta} U_{\mathbf{k}\mathbf{k}'\alpha\beta} \hat{c}_{\mathbf{k}+\frac{\mathbf{q}}{2}\alpha\uparrow}^\dagger \hat{c}_{-\mathbf{k}+\frac{\mathbf{q}}{2}\alpha\downarrow}^\dagger c_{-\mathbf{k}'+\frac{\mathbf{q}}{2}\beta\downarrow} c_{\mathbf{k}'+\frac{\mathbf{q}}{2}\beta\uparrow},$$

where $\alpha, \beta = \pm, 0$. Since the nearest-neighbor hopping hybridizes different orbitals, we assume the matrix elements of the on-site pairing interaction to be uniform, which yields a constant $U_{\mathbf{k}\mathbf{k}'\alpha\beta} = g < 0$, leading to a uniform order parameter $\Delta_\alpha = \Delta$ [41].

B. Pairing fluctuation theory

With the above Hamiltonian and dispersions of atomic Fermi gases in the Lieb lattice, we follow the pairing fluctuation theory previously developed for the pseudogap physics in the cuprates [10], which has been extended to address the BCS-BEC crossover in ultracold atomic Fermi gases [1]. This theory goes beyond the BCS mean-field approximation by self-consistently including finite momentum pairing correlations in the single particle self energy.

We recapitulate the formalism, extending it to the current multi-band situation. At finite T , the T -matrix $t(Q)$ contains a contribution from condensed pairs $t_{\text{sc}}(Q)$ and noncondensed pairs $t_{\text{pg}}(Q)$, where

$$t_{\text{sc}}(Q) = -\frac{\Delta_{\text{sc}}^2}{T} \delta(Q),$$

$$t_{\text{pg}}(Q) = \frac{g}{1 + g\chi(Q)}.$$

Here $K \equiv (\omega_n, \mathbf{k})$, $Q \equiv (\Omega_l, \mathbf{q})$, and ω_n (Ω_l) is the odd (even) Matsubara frequency. The pair susceptibility reads $\chi(Q) = -\sum_K \text{Tr}[G(K)\tilde{G}_0(K-Q)]$, with the full Green's function $G(K)$ and $\tilde{G}_0(K) = -G_0^T(-K)$, and the bare Green's function $G_0(K)$ is given by $G_0(K) = (i\omega - \hat{H}_{\mathbf{k}})^{-1}$. Thus, the self energy $\Sigma(K) = \Sigma_{\text{sc}}(K) + \Sigma_{\text{pg}}(K)$ contains two parts, where the Cooper pair condensate contribution $\Sigma_{\text{sc}}(K) = \Delta_{\text{sc}}^2 \tilde{G}_0(K)$ vanishes above T_c , and finite momentum pair contribution $\Sigma_{\text{pg}}(K) = -\sum_{Q \neq 0} t_{\text{pg}}(Q) \tilde{G}_0(K-Q)$ exists both above and below T_c .

According to the Thouless criteria [42], the condition for pairs to generate macroscopic occupation at zero momentum requires $1 + g\chi(0) = 0$, indicating that the main contribution to $\Sigma_{\text{pg}}(K)$ is concentrated in the vicinity of zero momentum for pairs. Therefore, we make the following approximation $\Sigma_{\text{pg}}(K) \approx \Delta_{\text{pg}}^2 \tilde{G}_0(K)$, thus define the pseudogap $\Delta_{\text{pg}}^2 = -\sum_{Q \neq 0} t_{\text{pg}}(Q)$. Then the total self-energy $\Sigma(K)$ takes the simple BCS-like form $\Sigma(K) = \Delta^2 \tilde{G}_0(K)$, where $\Delta^2 = \Delta_{\text{sc}}^2 + \Delta_{\text{pg}}^2$. Finally, the Dyson's equation leads immediately to the Green's function $G^{-1}(K) = G_0^{-1}(K) - \Delta^2 \tilde{G}_0(K)$.

Under the constraints $n = 2 \sum_K \text{Tr}G(K)$, we have the number equation

$$n = 2 \sum_{\mathbf{k}} \sum_{\alpha=0,\pm} \left[(v_{\mathbf{k}}^\alpha)^2 + \frac{\xi_{\mathbf{k}}^\alpha}{E_{\mathbf{k}}^\alpha} f(E_{\mathbf{k}}^\alpha) \right], \quad (1)$$

where $f(x)$ is the Fermi distribution function, $E_{\mathbf{k}}^\alpha = \sqrt{(\xi_{\mathbf{k}}^\alpha)^2 + \Delta^2}$, $(u_{\mathbf{k}}^\alpha)^2 = \frac{1}{2}(1 + \frac{\xi_{\mathbf{k}}^\alpha}{E_{\mathbf{k}}^\alpha})$, $(v_{\mathbf{k}}^\alpha)^2 = \frac{1}{2}(1 - \frac{\xi_{\mathbf{k}}^\alpha}{E_{\mathbf{k}}^\alpha})$. At $T \leq T_c$, the Thouless criteria, $1 + g\chi(0) = 0$, leads to the gap equation

$$0 = \frac{1}{g} + \sum_{\mathbf{k}} \sum_{\alpha=0,\pm} \frac{1 - 2f(E_{\mathbf{k}}^\alpha)}{2E_{\mathbf{k}}^\alpha}. \quad (2)$$

To evaluate the pseudogap, one can Taylor expand $t_{\text{pg}}^{-1}(Q)$ on the real frequency axis, after analytical continuation, $t_{\text{pg}}^{-1}(\Omega, \mathbf{q}) \approx a_1 \Omega^2 + a_0(\Omega - \Omega_{\mathbf{q}}^0 + \mu_p)$, with $\Omega_{\mathbf{q}}^0 = 2B(2 -$

$\cos q_x - \cos q_y) + 2B_z(1 - \cos q_z)$ and the effective pair chemical potential $\mu_p = 0$ at $T \leq T_c$. Here, B and B_z represent the in-plane and out-of-plane effective pair hopping integrals, respectively. B can be divided into conventional and geometric term, with $B = B_c + B_g$. And B_g is proportional to quantum metric of the upper or lower energy band. Consequently, we have the pseudogap equation

$$|a_0| \Delta_{\text{pg}}^2 = \sum_{\mathbf{q}} \left(1 + 4 \frac{a_1}{a_0} \Omega_{\mathbf{q}}^0 \right)^{-1/2} b(\Omega_{\mathbf{q}}), \quad (3)$$

where $b(x)$ is the Bose distribution function and $\Omega_{\mathbf{q}} = (\sqrt{a_0^2 + 4a_0a_1\Omega_{\mathbf{q}}^0} - a_0)/2a_1$ is the pair dispersion. As usual, here we have set $\hbar = k_B = 1$ and the volume V to unity [10].

Equations (1)-(3) form a closed set of self-consistent equations, which can be used to solve for $(\mu, \Delta_{\text{pg}}, T_c)$ with $\Delta_{\text{sc}} = 0$, and for $(\mu, \Delta, \Delta_{\text{pg}})$ at $T < T_c$. Here the order parameter Δ_{sc} can be derived from $\Delta_{\text{sc}}^2 = \Delta^2 - \Delta_{\text{pg}}^2$ below T_c .

C. Superfluid density

Superfluid density is a crucial transport property, which is correlated with condensed pairs. The low T dependence of superfluid density often provides insight into the symmetry of the pairing order. In the presence of a lattice, the superfluid density is determined by averaging the inverse band mass, which differs from the 3D continuum case where at zero temperature it is always given by the ratio of the particle density to the mass. Additionally, the in-plane component of the superfluid density can be decomposed into a conventional and geometric parts, owing to the presence of a flat band. The geometric term is influenced by the interband matrix elements of the current operator, which is directly proportional to the quantum metric.

The expressions for superfluid density are derived using the linear response theory within the BCS framework [43, 44], which is applied to the multi-band system [27]. Similar to Ref. [27], the in-plane superfluid density $(n_s/m)_{\parallel}$ contains a conventional term $(n_s/m)_{\parallel}^{\text{conv}}$ and a geometric term $(n_s/m)_{\parallel}^{\text{geom}}$, i.e.,

$$\left(\frac{n_s}{m} \right)_{\parallel} = \left(\frac{n_s}{m} \right)_{\parallel}^{\text{conv}} + \left(\frac{n_s}{m} \right)_{\parallel}^{\text{geom}}, \quad (4)$$

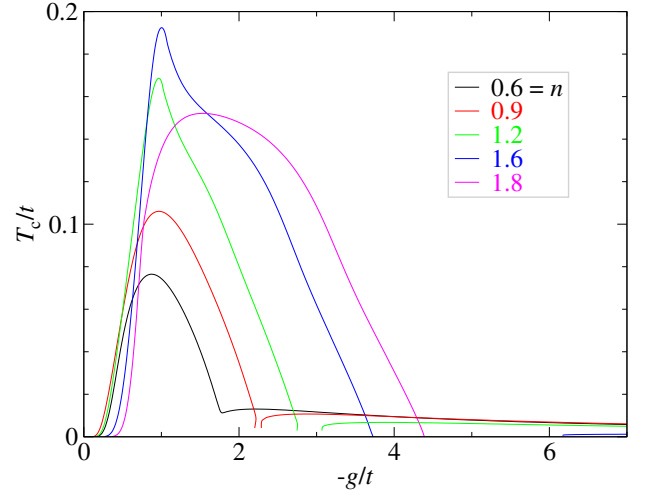


Figure 1. T_c as a function of $-g/t$ for $0.6 \leq n \leq 1.8$, with μ away from the flat band.

where

$$\begin{aligned} \left(\frac{n_s}{m} \right)_{\parallel}^{\text{conv}} &= \sum_{\mathbf{k}} \sum_{\alpha=\pm} \frac{t^2 \Delta_{\text{sc}}^2}{2E_{\mathbf{k}}^{\alpha 2}} \left[\frac{1 - 2f(E_{\mathbf{k}}^{\alpha})}{2E_{\mathbf{k}}^{\alpha}} + f'(E_{\mathbf{k}}^{\alpha}) \right] \\ &\quad \times \frac{\sin^2(k_x) + \sin^2(k_y)}{2 + \cos(k_x) + \cos(k_y)}, \end{aligned} \quad (5)$$

$$\begin{aligned} \left(\frac{n_s}{m} \right)_{\parallel}^{\text{geom}} &= 2 \sum_{\mathbf{k}} \Delta_{\text{sc}}^2 (g_{xx} + g_{yy}) \\ &\quad \times \left[\left(\frac{1 - 2f(E_{\mathbf{k}}^+)}{2E_{\mathbf{k}}^+} - \frac{1 - 2f(E_{\mathbf{k}})}{2E_{\mathbf{k}}} \right) \frac{\xi_{\mathbf{k}} - \xi_{\mathbf{k}}^+}{\xi_{\mathbf{k}} + \xi_{\mathbf{k}}^+} \right. \\ &\quad \left. + \left(\frac{1 - 2f(E_{\mathbf{k}}^-)}{2E_{\mathbf{k}}^-} - \frac{1 - 2f(E_{\mathbf{k}})}{2E_{\mathbf{k}}} \right) \frac{\xi_{\mathbf{k}} - \xi_{\mathbf{k}}^-}{\xi_{\mathbf{k}} + \xi_{\mathbf{k}}^-} \right]. \end{aligned} \quad (6)$$

Here $g_{\mu\nu} = \text{Re}(\partial_{\mu}\langle + | (1 - |+\rangle\langle +|) \partial_{\nu} |+\rangle)$ is the quantum metric tensor of the upper or the lower band, where $|\pm\rangle$ is the eigenvector of $\hat{H}_{\mathbf{k}}$, associated with the upper and lower free bands, respectively. The out-of-plane component reads

$$\left(\frac{n_s}{m} \right)_z = \sum_{\mathbf{k}} \sum_{\alpha=0,\pm} \frac{4t_z^2 \Delta_{\text{sc}}^2}{E_{\mathbf{k}}^{\alpha 2}} \left[\frac{1 - 2f(E_{\mathbf{k}}^{\alpha})}{2E_{\mathbf{k}}^{\alpha}} + f'(E_{\mathbf{k}}^{\alpha}) \right] \sin^2 k_z. \quad (7)$$

III. NUMERICAL RESULTS AND DISCUSSIONS

A. Effect of the flat band on T_c behaviors

We first investigate the behavior of the superfluid transition temperature for a range of $0.6 \leq n \leq 1.8$, when the Fermi level is located away from the flat band. As shown in Fig. 1, T_c follows the BCS solution in the weak-coupling regime and exhibits an exponential law due to the small pairing gap governed by the Bogoliubov excitation. As the interaction becomes stronger, the gap increases and the Fermi

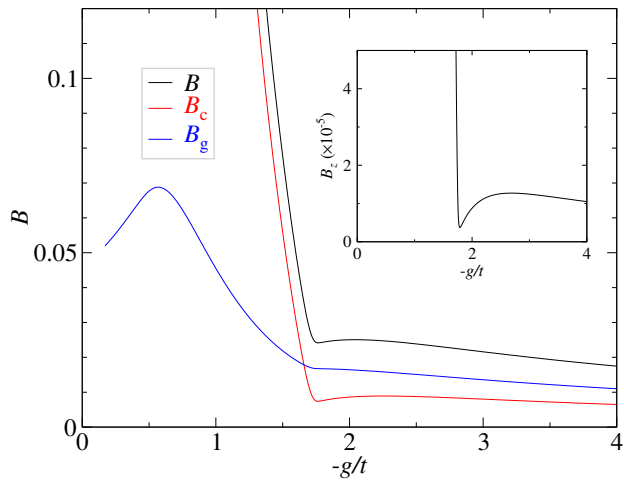


Figure 2. Evolution of the effective in-plane pair hopping integral B (black curve) along with its conventional (red curve) and geometric part (blue curve) as a function of $-g/t$ for $n = 0.6$. Shown in the inset is the corresponding out-of-plane pair hopping integral B_z .

surface shrinks. Consequently, the density of state (DOS) near the Fermi level decreases, resulting in a decreasing T_c after reaching a maximum in the unitary regime. For small $n = 0.6$, T_c reaches a minimum when $\mu = 0$, corresponding to a vanishing Fermi surface. At this point, the system enters the BEC regime and all fermions pair up. In the BEC regime, T_c initially rises due to the shrinking pair size but then decreases as the interaction increases towards the deep BEC region, influenced by the lattice effect.

Remarkably, for large n , T_c exhibits a reentrant behavior. After reaching a maximum, T_c decreases and completely vanishes in a range of intermediate coupling strengths before recovering as the interaction becomes stronger in the BEC regime. This is accompanied by the emergence of a PDW ground state where T_c vanishes. And similar PDW ground state has been found in a 3D lattice with high density [45] and a 2D optical lattice with strong lattice effect [39, 40], together with in the p -wave superfluid in dipolar Fermi gases [38]. The emergence of PDW states is a result of the strong repulsive inter-pair interaction and the relatively low kinetic energy of the pairs at relatively high densities. As the density increases, the repulsion between fermion pairs becomes stronger at intermediate and strong coupling, leading to a Wigner crystallization with a negative ξ^2 (or ξ_z^2). The range of interaction strength where the PDW state emerges extends with increasing n . In the PDW state, the minimum of the pair dispersion $\Omega_{\mathbf{q}}$ shifts from $\mathbf{q} = (0, 0, 0)$ to a nonzero \mathbf{q} . Although the PDW state has been experimentally observed, its ability to maintain superfluidity and thus form a supersolid remains to be studied. Moreover, in the BEC region, the superfluidity completely vanishes for high densities $n \geq 1.8$, similar to the case with a high density in the 3D lattice [45].

As is known, the superfluid transition temperature T_c in the BEC regime is mainly determined by the effective pair hopping integrals B and B_z . In Fig. 2, we present the behavior of the effective in-plane pair hopping integral B , as well as

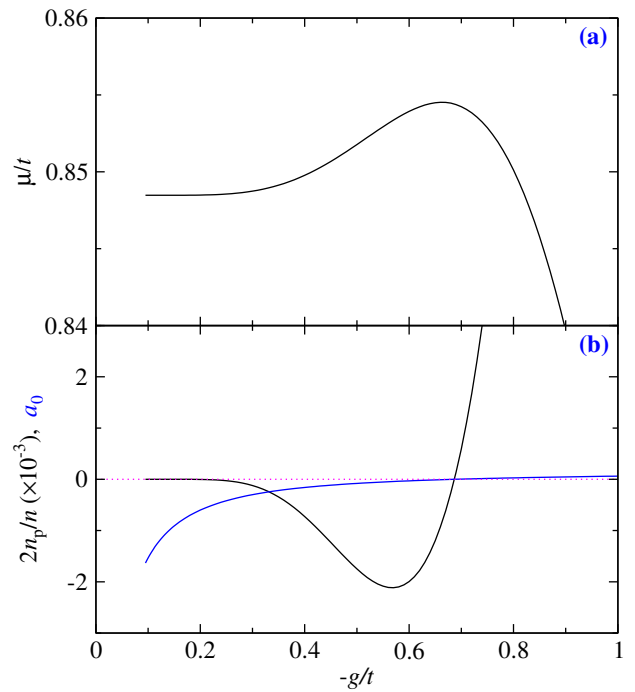


Figure 3. Behaviors of (a) μ and (b) $2n_p/n$ and a_0 as a function of $-g/t$ for $n = 1$.

its conventional component B_c and geometric component B_g , as a function of $-g/t$ for $n = 0.6$. The corresponding out-of-plane pair hopping integral B_z is shown in the inset. In the weak interaction regime, the size of the pairs is relatively large, causing significant overlap between pairs. This leads to highly collective pair motions and consequently large effective pair hopping integrals. Both B_c and B_z decrease as the size of the pairs gradually shrinks with increasing interaction strength, eventually reaching a minimum at $\mu = 0$ due to a stronger inter-pair repulsion. In the weak interaction regime, the geometric term B_g is negligible compared to B_c . As the interaction strength increases in the BEC regime, both B_c and B_z initially increase due to the decrease in repulsive interaction between pairs. However, they subsequently decrease towards the deep BEC region, where pair hopping is achieved through “virtual ionization” [46, 47], and the motion of pairs is strongly suppressed. Furthermore, the contribution of B_g becomes more significant than that of B_c in the BEC regime, which greatly enhances the superfluidity.

Shown in Fig. 3 is the behavior of μ in panel (a), along with $2n_p/n$ in panel (b), where $n_p = a_0 \Delta^2$, for $n = 1$ in the weak coupling region. The plot in panel (b) also includes a_0 . From panel (a), it can be observed that μ initially increases with increasing pairing strength, and exhibits a nonmonotonic behavior in the weak coupling BCS region. This behavior is similar to that for a 2D optical lattice with a strong lattice effect [39, 40], but differs from the counterparts in the 3D continuum and 3D lattice cases below half filling. In a quasi-two-dimensional Lieb lattice, the lower energy band possesses two van Hove singularities (VHS) at $\varepsilon = (2\sqrt{2} - 2)t \approx 0.8284t$ and $\varepsilon = (2\sqrt{2} - 2)t + 4t_z \approx 0.8684t$ as determined by

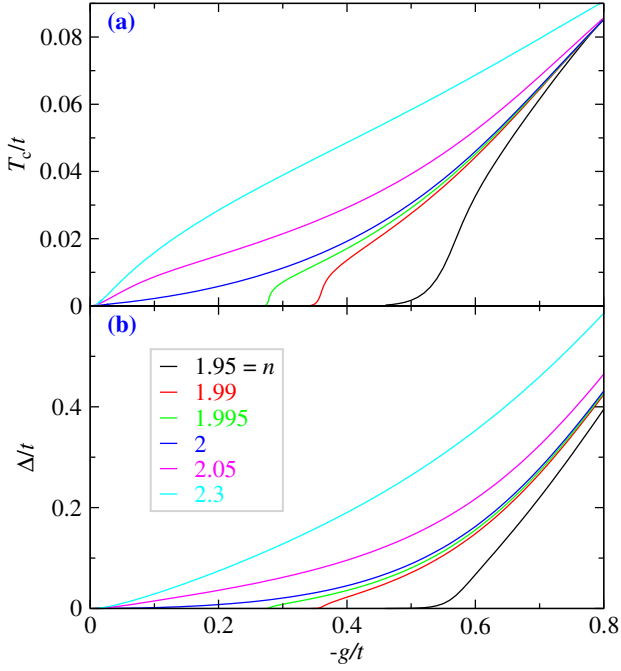


Figure 4. Behaviors of (a) T_c and (b) Δ as a function of $-g/t$ for large $1.95 \leq n \leq 2.3$ in the weak coupling BCS regime, with μ close to or inside the flat band.

$\nabla \xi_{\mathbf{k}}^\alpha = 0$. When μ exceeds $0.8684t$ in the weak coupling region, the DOS exhibits a negative slope as a function of ε , resulting in holelike pairing. This phenomenon can be explained by the general relation $n_p = n/2 - \sum_{\mathbf{k}\alpha} f(\xi_{\mathbf{k}}^\alpha)$, where n_p and $\sum_{\mathbf{k}\alpha} f(\xi_{\mathbf{k}}^\alpha)$ can be roughly understood as the densities of fermion pairs and free fermions, respectively. Within the holelike pairing regime, a_0 is negative (hence $n_p < 0$) as shown in panel (b), and $n_p (< 0)$ decreases (absolute value of n_p increases) with increasing interaction strength in the BCS regime, leading to an increase in the density of free fermions and causing μ to exceed its noninteracting value. As the pairing strength continues to increase, the contribution of the DOS below the VHS's becomes significant, causing μ to decrease again.

We present in Fig. 4 the behavior of (a) T_c and (b) Δ as a function of $-g/t$ for various densities near $n = 2$ in the weak coupling BCS region. For $n < 2$, both the T_c and Δ curves exhibit an exponential law in the weak coupling region, similar to the counterparts in the 3D continuum and 3D lattice case below half filling. However, as the density exceeds $n = 2$, the Fermi level enters the flat band with the lower band being fully occupied, resulting in a change in the behavior of both curves from an exponential law to an unusual power law. And the exponent in the power law is determined by the density. This change is a consequence of the large DOS of the flat band. To simplify the analysis, we treat the DOS of the flat band as a Dirac function due to the small broadening in the z direction, and average the DOSs of the upper and lower energy bands at extremely weak interactions, which yields $\bar{\Delta} \propto (n-2)|g|$ for $n > 2$ and $\bar{\Delta} \propto \exp(1/ng)$ for $n < 2$ in the weak coupling region, where $\bar{\Delta}$ is the leading order of Δ [29, 36]. Simi-

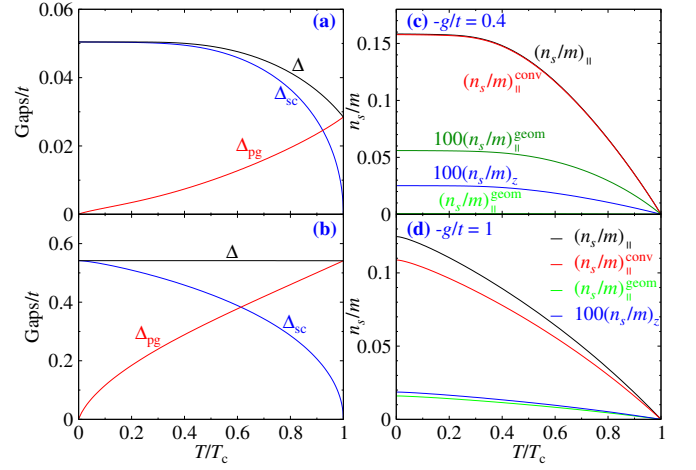


Figure 5. Behavior of the gaps, as labeled, as a function of T/T_c , for (a) $-g/t = 0.4$ and (b) 1 with $T_c/T_F = 0.02547$ and 0.07437 at $n = 0.6$, respectively. Plotted in (c-d) are the corresponding in-plane superfluid density $(n_s/m)_\parallel$ (black curves) along with its conventional (red curves) and geometric parts (green curves) for (c) $-g/t = 0.4$ and (d) 1, respectively. Also shown is $100(n_s/m)_z$ (blue curves) for clarity.

lar qualitative behavior of magnetism has been observed in a quasi two-dimensional repulsive Lieb lattice system at half filling [29]. In that case, the magnetism as a function of the interaction $U > 0$ also changes from an exponential law to a power law due to the influence of the flat band. Furthermore, under the particle-hole canonical transformation with $c_{i\uparrow}^\dagger \rightarrow c_{i\uparrow}^\dagger, c_{i\downarrow}^\dagger \rightarrow (-1)^i c_{i\downarrow}$, where i is the index of the site, the superconducting and charge order in the attractive model correspond to magnetic order in the repulsive model at half filling [48].

B. Gaps and superfluid densities in the superfluid phase

In Fig. 5, we plot the behavior of the order parameter Δ_{sc} , the pseudogap Δ_{pg} , and the total gap Δ . We also include the corresponding in-plane superfluid density $(n_s/m)_\parallel$, along with the conventional part $(n_s/m)_\parallel^{conv}$ and the geometric part $(n_s/m)_\parallel^{geom}$. The out-of-plane component of the superfluid density $(n_s/m)_z$ (blue $100\times$ magnified curves) is also shown for clarity. The results are for the case of $n = 0.6$ at $-g/t = 0.4$ and 1, as labeled, from top to bottom for the weak and strong coupling strengths, respectively.

Throughout the BCS-BEC crossover, both cases exhibit a pseudogap, similar to the regular 3D continuum case [44]. At zero temperature, all pairs are condensed, resulting in $\Delta_{pg} = 0$. As the temperature increases, the pairs are excited from zero momentum to finite momentum, leading to the onset of the pseudogap at $T = 0$. Concurrently, Δ_{sc} starts to decrease. When the temperature reaches T_c , the pairs are fully excited, resulting in $\Delta_{sc} = 0$ and $\Delta_{pg} = \Delta$. For the weak coupling case $-g/t = 0.4$ in panel (a), the total gap remains approximately constant in the low temperature re-

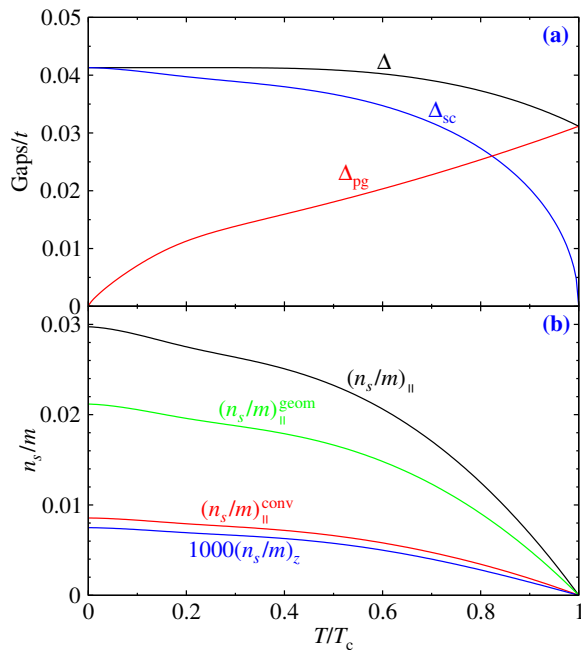


Figure 6. Evolution of (a) the gaps and (b) the superfluid densities, as labeled, as a function of T/T_c , at the weak coupling strength $-g/t = 0.1$ for $n = 2.4$, with μ located within the flat band.

gion. As the temperature further increases, the Bogoliubov quasiparticles dominates the excitation, leading to a decrease in Δ . The behavior of Δ_{sc} follows a BCS-like form and exhibits an exponential dependence on T , where Δ_{pg} is small. In panel (b), as the interaction strength increases to $-g/t = 1$, the bosonic pair excitation becomes dominant, and Δ_{pg} increases. The total gap Δ remains almost constant below T_c and becomes temperature independent in the strong coupling limit. The pseudogap Δ_{pg} follows a power law at low T , with $\Delta_{pg} \propto T^{3/4}$. Correspondingly, the behavior of Δ_{sc} transitions from an exponential law to a power law at low T .

In panel (c), the behavior of $(n_s/m)_{\parallel}$ as a function of T/T_c exhibits an exponential dependence on T in the low temperature region for $-g/t = 0.4$. When the interaction strength increases to $-g/t = 1$ in panel (d), $(n_s/m)_{\parallel}$ evolves from an exponential law to a power law. This is in contrast with the d-wave pairing case, where n_s/m has a linear dependence on T regardless of the interaction strength [10]. The temperature dependence of the out-of-plane superfluid density $(n_s/m)_z$ is similar to that of $(n_s/m)_{\parallel}$, as can be seen more clearly from the (blue) 100 \times magnified curves. This is because both $(n_s/m)_{\parallel}$ and $(n_s/m)_z$ are mainly governed by the prefactor Δ_{sc}^2 . However, $(n_s/m)_z$ is strongly suppressed due to the small out-of-plane dispersion with $t_z/t = 0.01$. Furthermore, $(n_s/m)_{\parallel}$ contains contributions from both $(n_s/m)_{\parallel}^{conv}$ and $(n_s/m)_{\parallel}^{geom}$, with the former remaining finite while the latter approaches zero as the interaction decreases. In the weak coupling region, when μ is far away from the flat band, the ge-

ometric part $(n_s/m)_{\parallel}^{geom}$ exhibits an exponential dependence on $-g/t$. Consequently, the contribution from $(n_s/m)_{\parallel}^{geom}$ gradually decreases as the interaction decreases.

Finally, we investigate the effects of the flat band on the gaps and superfluid densities in the superfluid phase, when the Fermi level enters into the flat band for $n \geq 2$ in the weak coupling region. The results are shown in Fig. 6 for $n = 2.4$ and $-g/t = 0.1$, where various gaps and the components of superfluid density are plotted as a function of T/T_c . Compared with the weak coupling case in panel (a) of Fig. 5, the behavior of Δ_{pg} exhibits a power law dependence on T in the low temperature region, despite its small value due to the extremely weak interaction. As a consequence, the dependence of Δ_{sc} on T changes from an exponential law to a power law at low T under the influence of the flat band. Moreover, both $(n_s/m)_{\parallel}$ and $(n_s/m)_z$ show a power law dependence on T , governed by Δ_{sc} . Notably, at low T , $(n_s/m)_{\parallel}^{geom}$ contributes more to the in-plane superfluid density compared to $(n_s/m)_{\parallel}^{conv}$.

IV. CONCLUSIONS

In summary, we have conducted a comprehensive study on the impact of the flat band on the superfluidity and pairing phenomena of a Fermi gas in a quasi-2D Lieb lattice within the framework of BCS-BEC crossover at finite temperature. Our investigation has revealed the presence of quantum geometric effects in the Lieb lattice, manifested by the enhanced effective pair hopping integral and superfluid densities, which contribute significantly to the superfluidity. Especially, when the Fermi level resides within the flat band, the pairing gap and the superfluid transition temperature exhibit an unusual power law behavior in the weak coupling regime, as a function of the interaction strength. Meanwhile, in the low temperature regime, we find that the order parameter, pseudogap, and superfluid densities in the superfluid phase display an anomalous power law dependence. Additionally, as the chemical potential surpasses the van Hove singularities in the lower band from below, the pairing undergoes a transition to a holelike behavior for weak interactions, resulting in a non-monotonic variation of the chemical potential versus the interaction strength. In particular, in the case of relatively high density, a PDW ground state emerges within a finite range of intermediate pairing strength, owing to the presence of strong interpair repulsive interaction and large pair size. These intriguing findings for the Lieb lattice exhibit stark contrast to that for pure 3D continuum and 3D cubic lattices, underscoring the need for future experimental test.

V. ACKNOWLEDGMENTS

This work was supported by the Innovation Program for Quantum Science and Technology (Grant No. 2021ZD0301904).

Appendix A: Coefficients of the Taylor-expanded inverse T -matrix

In this Appendix, we present concrete expressions for the coefficients of the Taylor expansion of the inverse T -matrix, $t(\Omega, \mathbf{q})$, after analytical continuation,

$$t_{pg}^{-1}(\mathbf{q}, \Omega) = a_1 \Omega^2 + a_0 (\Omega - \Omega_{\mathbf{q}} + \mu_p). \quad (\text{A1})$$

Here $\mu_p = t^{-1}(0, 0)/a_0$, which vanishes for $T \leq T_c$. In the long wavelength limit,

$$\Omega_{\mathbf{q}} = Bq_x^2 + Bq_y^2 + B_z q_z^2 \equiv \frac{q_x^2}{2M^*} + \frac{q_y^2}{2M^*} + \frac{q_z^2}{2M_z^*}, \quad (\text{A2})$$

with $B = 1/2M^*$ and $B_z = 1/2M_z^*$, in which M^*, M_z^* correspond to the in-plane and out-of-plane effective pair mass, respectively.

Before expansion, the inverse T matrix is given by

$$t_{\mathbf{q}, \Omega + i0^+}^{-1} = U^{-1} + \chi(\mathbf{q}, \Omega + i0^+), \quad (\text{A3})$$

with pair susceptibility $\chi(Q) = -\sum_K \text{Tr}[G_\sigma(K) \tilde{G}_{0, \bar{\sigma}}(K - Q)]$, where G and G_0 cannot be diagnosed simultaneously when $Q \neq 0$. After analytical continuation $i\Omega_n \rightarrow \Omega + i0^+$, $\chi(\mathbf{q}, \Omega + i0^+)$ reads

$$\begin{aligned} \chi(\mathbf{q}, \Omega + i0^+) = & \sum_{\mathbf{k}} \left(\frac{1 - f(E_{\mathbf{k}}) - f(\xi_{\mathbf{q}-\mathbf{k}})}{E_{\mathbf{k}} + \xi_{\mathbf{q}-\mathbf{k}} - \Omega - i0^+} u_{\mathbf{k}}^2 - \frac{f(E_{\mathbf{k}}) - f(\xi_{\mathbf{q}-\mathbf{k}})}{E_{\mathbf{k}} - \xi_{\mathbf{q}-\mathbf{k}} + \Omega + i0^+} v_{\mathbf{k}}^2 \right) \Gamma_{\mathbf{q}, \mathbf{k}}^2 + \\ & \left(\frac{1 - f(E_{\mathbf{k}}) - f(\xi_{\mathbf{q}-\mathbf{k}}^+)}{E_{\mathbf{k}} + \xi_{\mathbf{q}-\mathbf{k}}^+ - \Omega - i0^+} u_{\mathbf{k}}^2 - \frac{f(E_{\mathbf{k}}) - f(\xi_{\mathbf{q}-\mathbf{k}}^+)}{E_{\mathbf{k}} - \xi_{\mathbf{q}-\mathbf{k}}^+ + \Omega + i0^+} v_{\mathbf{k}}^2 \right) \frac{1}{2} (1 - \Gamma_{\mathbf{q}, \mathbf{k}}^2) + \\ & \left(\frac{1 - f(E_{\mathbf{k}}) - f(\xi_{\mathbf{q}-\mathbf{k}}^-)}{E_{\mathbf{k}} + \xi_{\mathbf{q}-\mathbf{k}}^- - \Omega - i0^+} u_{\mathbf{k}}^2 - \frac{f(E_{\mathbf{k}}) - f(\xi_{\mathbf{q}-\mathbf{k}}^-)}{E_{\mathbf{k}} - \xi_{\mathbf{q}-\mathbf{k}}^- + \Omega + i0^+} v_{\mathbf{k}}^2 \right) \frac{1}{2} (1 - \Gamma_{\mathbf{q}, \mathbf{k}}^2) + \\ & \left(\frac{1 - f(E_{\mathbf{k}}^+) - f(\xi_{\mathbf{q}-\mathbf{k}})}{E_{\mathbf{k}}^+ + \xi_{\mathbf{q}-\mathbf{k}} - \Omega - i0^+} (u_{\mathbf{k}}^+)^2 - \frac{f(E_{\mathbf{k}}^+) - f(\xi_{\mathbf{q}-\mathbf{k}})}{E_{\mathbf{k}}^+ - \xi_{\mathbf{q}-\mathbf{k}} + \Omega + i0^+} (v_{\mathbf{k}}^+)^2 \right) \frac{1}{2} (1 - \Gamma_{\mathbf{q}, \mathbf{k}}^2) + \\ & \left(\frac{1 - f(E_{\mathbf{k}}^+) - f(\xi_{\mathbf{q}-\mathbf{k}}^+)}{E_{\mathbf{k}}^+ + \xi_{\mathbf{q}-\mathbf{k}}^+ - \Omega - i0^+} (u_{\mathbf{k}}^+)^2 - \frac{f(E_{\mathbf{k}}^+) - f(\xi_{\mathbf{q}-\mathbf{k}}^+)}{E_{\mathbf{k}}^+ - \xi_{\mathbf{q}-\mathbf{k}}^+ + \Omega + i0^+} (v_{\mathbf{k}}^+)^2 \right) \frac{1}{4} (1 + \Gamma_{\mathbf{q}, \mathbf{k}}^2) + \\ & \left(\frac{1 - f(E_{\mathbf{k}}^+) - f(\xi_{\mathbf{q}-\mathbf{k}}^-)}{E_{\mathbf{k}}^+ + \xi_{\mathbf{q}-\mathbf{k}}^- - \Omega - i0^+} (u_{\mathbf{k}}^+)^2 - \frac{f(E_{\mathbf{k}}^+) - f(\xi_{\mathbf{q}-\mathbf{k}}^-)}{E_{\mathbf{k}}^+ - \xi_{\mathbf{q}-\mathbf{k}}^- + \Omega + i0^+} (v_{\mathbf{k}}^+)^2 \right) \frac{1}{4} (1 - \Gamma_{\mathbf{q}, \mathbf{k}}^2) + \\ & \left(\frac{1 - f(E_{\mathbf{k}}^-) - f(\xi_{\mathbf{q}-\mathbf{k}})}{E_{\mathbf{k}}^- + \xi_{\mathbf{q}-\mathbf{k}} - \Omega - i0^+} (u_{\mathbf{k}}^-)^2 - \frac{f(E_{\mathbf{k}}^-) - f(\xi_{\mathbf{q}-\mathbf{k}})}{E_{\mathbf{k}}^- - \xi_{\mathbf{q}-\mathbf{k}} + \Omega + i0^+} (v_{\mathbf{k}}^-)^2 \right) \frac{1}{2} (1 - \Gamma_{\mathbf{q}, \mathbf{k}}^2) + \\ & \left(\frac{1 - f(E_{\mathbf{k}}^-) - f(\xi_{\mathbf{q}-\mathbf{k}}^+)}{E_{\mathbf{k}}^- + \xi_{\mathbf{q}-\mathbf{k}}^+ - \Omega - i0^+} (u_{\mathbf{k}}^-)^2 - \frac{f(E_{\mathbf{k}}^-) - f(\xi_{\mathbf{q}-\mathbf{k}}^+)}{E_{\mathbf{k}}^- - \xi_{\mathbf{q}-\mathbf{k}}^+ + \Omega + i0^+} (v_{\mathbf{k}}^-)^2 \right) \frac{1}{4} (1 - \Gamma_{\mathbf{q}, \mathbf{k}}^2) + \\ & \left(\frac{1 - f(E_{\mathbf{k}}^-) - f(\xi_{\mathbf{q}-\mathbf{k}}^-)}{E_{\mathbf{k}}^- + \xi_{\mathbf{q}-\mathbf{k}}^- - \Omega - i0^+} (u_{\mathbf{k}}^-)^2 - \frac{f(E_{\mathbf{k}}^-) - f(\xi_{\mathbf{q}-\mathbf{k}}^-)}{E_{\mathbf{k}}^- - \xi_{\mathbf{q}-\mathbf{k}}^- + \Omega + i0^+} (v_{\mathbf{k}}^-)^2 \right) \frac{1}{4} (1 + \Gamma_{\mathbf{q}, \mathbf{k}}^2), \end{aligned} \quad (\text{A4})$$

where

$$\Gamma_{\mathbf{q}, \mathbf{k}} = \frac{2 \cos \frac{1}{2} k_x \cos \frac{1}{2} (q_x - k_x) + 2 \cos \frac{1}{2} k_y \cos \frac{1}{2} (q_y - k_y)}{\sqrt{2 + \cos k_x + \cos k_y} \sqrt{2 + \cos (q_x - k_x) + \cos (q_y - k_y)}} = \hat{h}_{\mathbf{k}} \cdot \hat{h}_{\mathbf{q}-\mathbf{k}}$$

which gives $\Gamma_{\mathbf{q}, \mathbf{k}}|_{\mathbf{q}=0} = 1$, $\partial_\mu \Gamma_{\mathbf{q}, \mathbf{k}}|_{\mathbf{q}=0} = 0$, and $\partial_\mu \partial_\nu \Gamma_{\mathbf{q}, \mathbf{k}}|_{\mathbf{q}=0} = -2g_{\mu\nu}$. Here $g_{\mu\nu} = \text{Re}(\partial_\mu \langle + |) (1 - | + \rangle \langle + |) \partial_\nu | + \rangle = \frac{1}{2} \partial_\mu \hat{h}_{\mathbf{k}} \cdot \partial_\nu \hat{h}_{\mathbf{k}}$ is the quantum metric tensor of the upper or the lower band, where $|\pm\rangle = [\pm 1/\sqrt{2}, h_x/\sqrt{2}, h_y/\sqrt{2}]^T$ and $|0\rangle = [0, -h_y, h_x]^T$ with $\hat{h}_{\mathbf{k}} = [h_x, h_y]^T = [\cos(k_x/2)/\sqrt{\cos(k_x/2)^2 + \cos(k_y/2)^2}, \cos(k_y/2)/\sqrt{\cos(k_x/2)^2 + \cos(k_y/2)^2}]^T$.

a_0 and a_1 correspond to the first and second order expansion terms of the frequency of the inverse T -matrix, respectively. The a_1 term serves as a small quantitative correction in the BEC regime, where $a_1 T_c \ll a_0$. And we have

$$a_0 = \frac{1}{2\Delta^2} \left[n - 2 \sum_{\mathbf{k}} \sum_{\alpha=0,\pm} f(\xi_{\mathbf{k}}^\alpha) \right], \quad (\text{A5})$$

$$a_1 = \frac{1}{2\Delta^4} \sum_{\mathbf{k}} \sum_{\alpha=0,\pm} E_{\mathbf{k}}^\alpha \left[\left(1 + \frac{(\xi_{\mathbf{k}}^\alpha)^2}{(E_{\mathbf{k}}^\alpha)^2} \right) (1 - 2f(E_{\mathbf{k}}^\alpha)) - 2 \frac{\xi_{\mathbf{k}}^\alpha}{E_{\mathbf{k}}^\alpha} (1 - 2f(\xi_{\mathbf{k}}^\alpha)) \right]. \quad (\text{A6})$$

The pair dispersion coefficients are given by

$$B_i = \frac{1}{2} \left. \frac{\partial^2 \Omega_{\mathbf{q}}}{\partial q_i^2} \right|_{\mathbf{q}=\mathbf{0}} \quad (\text{A7})$$

B can be divided into a conventional and a geometric term, with $B = B_c + B_g$. where

$$B_c = -\frac{1}{4a_0\Delta^2} \sum_{\mathbf{k}} \sum_{\alpha=\pm} \left\{ \left[2f'(\xi_{\mathbf{k}}^\alpha) + \frac{E_{\mathbf{k}}^\alpha}{\Delta^2} \left[\left(1 + \frac{(\xi_{\mathbf{k}}^\alpha)^2}{(E_{\mathbf{k}}^\alpha)^2} \right) [1 - 2f(E_{\mathbf{k}}^\alpha)] - 2 \frac{\xi_{\mathbf{k}}^\alpha}{E_{\mathbf{k}}^\alpha} [1 - 2f(\xi_{\mathbf{k}}^\alpha)] \right] \right] \right. \\ \left. \times (\nabla \xi_{\mathbf{k}}^\alpha)^2 - \frac{1}{2} \left[[1 - 2f(E_{\mathbf{k}}^\alpha)] - \frac{\xi_{\mathbf{k}}^\alpha}{E_{\mathbf{k}}^\alpha} [1 - 2f(\xi_{\mathbf{k}}^\alpha)] \right] \nabla^2 \xi_{\mathbf{k}}^\alpha \right\}, \quad (\text{A8})$$

with

$$\nabla^2 \xi_{\mathbf{k}}^\pm = \mp \frac{\sqrt{2}}{2} t \left(\frac{\cos k_x + \cos k_y}{\sqrt{2 + \cos k_x + \cos k_y}} + \frac{\sin^2 k_x + \sin^2 k_y}{2(2 + \cos k_x + \cos k_y)^{3/2}} \right), \\ (\nabla \xi_{\mathbf{k}}^\pm)^2 = \frac{t^2}{2} \frac{\sin^2 k_x + \sin^2 k_y}{2 + \cos k_x + \cos k_y},$$

and

$$B_g = -\frac{1}{4a_0} \sum_{\mathbf{k}} \left\{ -4 \left(\frac{1 - f(E_{\mathbf{k}}) - f(\xi_{\mathbf{k}})}{E_{\mathbf{k}} + \xi_{\mathbf{k}}} u_{\mathbf{k}}^2 - \frac{f(E_{\mathbf{k}}) - f(\xi_{\mathbf{k}})}{E_{\mathbf{k}} - \xi_{\mathbf{k}}} v_{\mathbf{k}}^2 \right) \right. \\ + 2 \left(\frac{1 - f(E_{\mathbf{k}}) - f(\xi_{\mathbf{k}}^+)}{E_{\mathbf{k}} + \xi_{\mathbf{k}}^+} u_{\mathbf{k}}^2 - \frac{f(E_{\mathbf{k}}) - f(\xi_{\mathbf{k}}^+)}{E_{\mathbf{k}} - \xi_{\mathbf{k}}^+} v_{\mathbf{k}}^2 \right) \\ + 2 \left(\frac{1 - f(E_{\mathbf{k}}) - f(\xi_{\mathbf{k}}^-)}{E_{\mathbf{k}} + \xi_{\mathbf{k}}^-} u_{\mathbf{k}}^2 - \frac{f(E_{\mathbf{k}}) - f(\xi_{\mathbf{k}}^-)}{E_{\mathbf{k}} - \xi_{\mathbf{k}}^-} v_{\mathbf{k}}^2 \right) \\ + 2 \left(\frac{1 - f(E_{\mathbf{k}}^+) - f(\xi_{\mathbf{k}})}{E_{\mathbf{k}}^+ + \xi_{\mathbf{k}}} (u_{\mathbf{k}}^+)^2 - \frac{f(E_{\mathbf{k}}^+) - f(\xi_{\mathbf{k}})}{E_{\mathbf{k}}^+ - \xi_{\mathbf{k}}} (v_{\mathbf{k}}^+)^2 \right) \\ - 2 \left(\frac{1 - f(E_{\mathbf{k}}^+) - f(\xi_{\mathbf{k}}^+)}{E_{\mathbf{k}}^+ + \xi_{\mathbf{k}}^+} (u_{\mathbf{k}}^+)^2 - \frac{f(E_{\mathbf{k}}^+) - f(\xi_{\mathbf{k}}^+)}{E_{\mathbf{k}}^+ - \xi_{\mathbf{k}}^+} (v_{\mathbf{k}}^+)^2 \right) \\ + 2 \left(\frac{1 - f(E_{\mathbf{k}}^-) - f(\xi_{\mathbf{k}})}{E_{\mathbf{k}}^- + \xi_{\mathbf{k}}} (u_{\mathbf{k}}^-)^2 - \frac{f(E_{\mathbf{k}}^-) - f(\xi_{\mathbf{k}})}{E_{\mathbf{k}}^- - \xi_{\mathbf{k}}} (v_{\mathbf{k}}^-)^2 \right) \\ \left. - 2 \left(\frac{1 - f(E_{\mathbf{k}}^-) - f(\xi_{\mathbf{k}}^-)}{E_{\mathbf{k}}^- + \xi_{\mathbf{k}}^-} (u_{\mathbf{k}}^-)^2 - \frac{f(E_{\mathbf{k}}^-) - f(\xi_{\mathbf{k}}^-)}{E_{\mathbf{k}}^- - \xi_{\mathbf{k}}^-} (v_{\mathbf{k}}^-)^2 \right) \right\} (g_{xx} + g_{yy}). \quad (\text{A9})$$

And B_z reads

$$B_z = -\frac{1}{2a_0\Delta^2} \sum_{\mathbf{k}} \sum_{\alpha=0,\pm} \left\{ \left[2f'(\xi_{\mathbf{k}}^\alpha) + \frac{E_{\mathbf{k}}^\alpha}{\Delta^2} \left[\left(1 + \frac{(\xi_{\mathbf{k}}^\alpha)^2}{(E_{\mathbf{k}}^\alpha)^2} \right) [1 - 2f(E_{\mathbf{k}}^\alpha)] - 2 \frac{\xi_{\mathbf{k}}^\alpha}{E_{\mathbf{k}}^\alpha} [1 - 2f(\xi_{\mathbf{k}}^\alpha)] \right] \right] \right. \\ \left. \times 4t_z^2 \sin^2 k_z - \frac{1}{2} \left[[1 - 2f(E_{\mathbf{k}}^\alpha)] - \frac{\xi_{\mathbf{k}}^\alpha}{E_{\mathbf{k}}^\alpha} [1 - 2f(\xi_{\mathbf{k}}^\alpha)] \right] 2t_z \cos k_z \right\} \quad (\text{A10})$$

- [2] I. Bloch, J. Dalibard, and W. Zwerger, Many-body physics with ultracold gases, *Rev. Mod. Phys.* **80**, 885 (2008).
- [3] W. Zwerger, *The BCS-BEC crossover and the unitary Fermi gas*, Vol. 836 (Springer Science & Business Media, 2011).
- [4] B. DeMarco and D. S. Jin, Onset of Fermi Degeneracy in a Trapped Atomic Gas, *Science* **285**, 1703 (1999).
- [5] M. Bartenstein, A. Altmeyer, S. Riedl, S. Jochim, C. Chin, J. H. Denschlag, and R. Grimm, Crossover from a molecular Bose-Einstein condensate to a degenerate Fermi gas, *Phys. Rev. Lett.* **92**, 120401 (2004).
- [6] M. Zwierlein, A. Schirotzek, C. Schunck, and W. Ketterle, Fermionic superfluidity with imbalanced spin populations, *Science* **311**, 492 (2006).
- [7] G. Partridge, W. Li, R. Kamar, Y. Liao, and R. Hulet, Pairing and phase separation in a polarized Fermi gas, *Science* **311**, 503 (2006).
- [8] C. Chin, R. Grimm, P. Julienne, and E. Tiesinga, Feshbach resonances in ultracold gases, *Rev. Mod. Phys.* **82**, 1225 (2010).
- [9] D. Jaksch, C. Bruder, J. I. Cirac, C. W. Gardiner, and P. Zoller, Cold bosonic atoms in optical lattices, *Phys. Rev. Lett.* **81**, 3108 (1998).
- [10] Q. J. Chen, I. Kosztin, B. Jankó, and K. Levin, Pairing fluctuation theory of superconducting properties in underdoped to overdoped cuprates, *Phys. Rev. Lett.* **81**, 4708 (1998).
- [11] R. A. Hart, P. M. Duarte, T.-L. Yang, X. Liu, T. Paiva, E. Khatami, R. T. Scalettar, N. Trivedi, D. A. Huse, and R. G. Hulet, Observation of antiferromagnetic correlations in the Hubbard model with ultracold atoms, *Nature* **519**, 211+ (2015).
- [12] I. Bloch, Quantum coherence and entanglement with ultracold atoms in optical lattices, *Nature* **453**, 1016 (2008).
- [13] Y. Cao, V. Fatemi, S. Fang, K. Watanabe, T. Taniguchi, E. Kaxiras, and P. Jarillo-Herrero, Unconventional superconductivity in magic-angle graphene superlattices, *Nature* **556**, 43 (2018).
- [14] N. B. Kopnin, T. T. Heikkilä, and G. E. Volovik, High-temperature surface superconductivity in topological flat-band systems, *Phys. Rev. B* **83**, 220503(R) (2011).
- [15] V. J. Kauppila, F. Aikebaier, and T. T. Heikkilä, Flat-band superconductivity in strained Dirac materials, *Phys. Rev. B* **93**, 214505 (2016).
- [16] Y.-F. Wang, Z.-C. Gu, C.-D. Gong, and D. N. Sheng, Fractional quantum hall effect of hard-core bosons in topological flat bands, *Phys. Rev. Lett.* **107**, 146803 (2011).
- [17] W. Beugeling, J. C. Everts, and C. Morais Smith, Topological phase transitions driven by next-nearest-neighbor hopping in two-dimensional lattices, *Phys. Rev. B* **86**, 195129 (2012).
- [18] E. H. Lieb, Two theorems on the Hubbard model, *Phys. Rev. Lett.* **62**, 1201 (1989).
- [19] K. Sun, Z. Gu, H. Katsura, and S. Das Sarma, Nearly flatbands with nontrivial topology, *Phys. Rev. Lett.* **106**, 236803 (2011).
- [20] E. Tang, J.-W. Mei, and X.-G. Wen, High-temperature fractional quantum hall states, *Phys. Rev. Lett.* **106**, 236802 (2011).
- [21] T. Neupert, L. Santos, C. Chamon, and C. Mudry, Fractional quantum hall states at zero magnetic field, *Phys. Rev. Lett.* **106**, 236804 (2011).
- [22] S. Taie, H. Ozawa, T. Ichinose, T. Nishio, S. Nakajima, and Y. Takahashi, Coherent driving and freezing of bosonic matter wave in an optical Lieb lattice, *Sci. Adv.* **1**, 10.1126/sciadv.1500854 (2015).
- [23] F. Schafer, T. Fukuhara, S. Sugawa, Y. Takasu, and Y. Takahashi, Tools for quantum simulation with ultracold atoms in optical lattices, *Nat. Rev. Phys.* **2**, 411 (2020).
- [24] K.-E. Huhtinen, M. Tylutki, P. Kumar, T. I. Vanhala, S. Peotta, and P. Törmä, Spin-imbalanced pairing and Fermi surface deformation in flat bands, *Phys. Rev. B* **97**, 214503 (2018).
- [25] B. Cui, X. Zheng, J. Wang, D. Liu, S. Xie, and B. Huang, Realization of Lieb lattice in covalent-organic frameworks with tunable topology and magnetism, *Nat. Commun.* **11**, 66 (2020).
- [26] G. Palumbo and K. Meichanetzidis, Two-dimensional Chern semimetals on the Lieb lattice, *Phys. Rev. B* **92**, 235106 (2015).
- [27] L. Liang, T. I. Vanhala, S. Peotta, T. Siro, A. Harju, and P. Törmä, Band geometry, Berry curvature, and superfluid weight, *Phys. Rev. B* **95**, 024515 (2017).
- [28] K. Noda, A. Koga, N. Kawakami, and T. Prusckke, Ferromagnetism of cold fermions loaded into a decorated square lattice, *Phys. Rev. A* **80**, 063622 (2009).
- [29] K. Noda, K. Inaba, and M. Yamashita, Magnetism in the three-dimensional layered Lieb lattice: Enhanced transition temperature via flat-band and Van Hove singularities, *Phys. Rev. A* **91**, 063610 (2015).
- [30] W. Nie, D. Zhang, and W. Zhang, Ferromagnetic ground state of the SU(3) Hubbard model on the Lieb lattice, *Phys. Rev. A* **96**, 053616 (2017).
- [31] N. Swain and M. Karmakar, Strain-induced superconductor-insulator transition on a Lieb lattice, *Phys. Rev. Res.* **2**, 023136 (2020).
- [32] V. I. Iglovikov, F. Hébert, B. Grémaud, G. G. Batrouni, and R. T. Scalettar, Superconducting transitions in flat-band systems, *Phys. Rev. B* **90**, 094506 (2014).
- [33] W. Zhu, S. Hou, Y. Long, H. Chen, and J. Ren, Simulating quantum spin hall effect in the topological Lieb lattice of a linear circuit network, *Phys. Rev. B* **97**, 075310 (2018).
- [34] E. Sadeghi and H. Rezania, Spin-orbit coupling effects on transport properties of electronic Lieb lattice in the presence of magnetic field, *Sci. Rep.* **12**, 10.1038/s41598-022-12588-5 (2022).
- [35] A. Pires, Transport on the ferromagnetic Lieb lattice, *J. Magn. Mater.* **547**, 168941 (2022).
- [36] H. Deng, C. P. Li, Y. X. Wu, L. Sun, and Q. J. Chen, Flat band effects on the ground-state BCS-BEC crossover in atomic Fermi gases in a quasi-two-dimensional Lieb lattice (2023), arXiv:2310.12944 [cond-mat.quant-gas].
- [37] L. Chen, T. Mazaheri, A. Seidel, and X. Tang, The impossibility of exactly flat non-trivial Chern bands in strictly local periodic tight binding models, *J. Phys. A: Math. Theor.* **47**, 152001 (2014).
- [38] Y. M. Che, J. B. Wang, and Q. J. Chen, Reentrant superfluidity and pair density wave in single-component dipolar Fermi gases, *Phys. Rev. A* **93**, 063611 (2016).
- [39] L. Sun, J. B. Wang, X. Chu, and Q. J. Chen, Pairing phenomena and superfluidity of atomic Fermi gases in a two-dimensional optical lattice: Unusual effects of lattice-continuum mixing, *Annalen der Physik* **534**, 2100511 (2022).
- [40] L. Sun and Q. J. Chen, Ground states of atomic Fermi gases in a two-dimensional optical lattice with and without population imbalance, *Phys. Rev. A* **106**, 013317 (2022).
- [41] N. Chamel, S. Goriely, J. M. Pearson, and M. Onsi, Unified description of neutron superfluidity in the neutron-star crust with analogy to anisotropic multiband BCS superconductors, *Phys. Rev. C* **81**, 045804 (2010).
- [42] D. J. Thouless, Perturbation theory in statistical mechanics and the theory of superconductivity, *Annals of Physics* **10**, 553 (1960).
- [43] D. J. Scalapino, S. R. White, and S. C. Zhang, Superfluid density and the drude weight of the hubbard model, *Phys. Rev. Lett.* **68**, 2830 (1992).
- [44] I. Kosztin, Q. J. Chen, B. Jankó, and K. Levin, Relationship between the pseudo- and superconducting gaps: Effects of residual pairing correlations below T_c , *Phys. Rev. B* **58**, R5936

- (1998).
- [45] C.-C. Chien, Q. J. Chen, and K. Levin, Fermions with attractive interactions on optical lattices and implications for correlated systems, *Phys. Rev. A* **78**, 043612 (2008).
- [46] P. Nozières and S. Schmitt-Rink, Bose condensation in an attractive fermion gas: from weak to strong coupling superconductivity, *J. Low Temp. Phys.* **59**, 195 (1985).
- [47] Q. J. Chen, I. Kosztin, B. Jankó, and K. Levin, Superconducting transitions from the pseudogap state: d-wave symmetry, lattice, and low-dimensional effects, *Phys. Rev. B* **59**, 7083 (1999).
- [48] R. T. Scalettar, E. Y. Loh, J. E. Gubernatis, A. Moreo, S. R. White, D. J. Scalapino, R. L. Sugar, and E. Dagotto, Phase diagram of the two-dimensional negative- U Hubbard model, *Phys. Rev. Lett.* **62**, 1407 (1989).